

Exploring Multi-physics with Extremely Weak Supervision

Shihang Feng¹ Peng Jin¹ Yinpeng Chen² Xitong Zhang¹ Zicheng Liu² Youzuo Lin¹

Abstract

Multi-physical inversion plays a critical role in geophysics. It has been widely used to infer various physical properties (such as velocity and conductivity), simultaneously. Among those inversion problems, some are explicitly governed by partial differential equations (PDEs), while others are not. Without explicit governing equations, conventional multi-physical inversion techniques will not be feasible and data-driven inversion require expensive full labels. To overcome this issue, we develop a new data-driven multi-physics inversion technique with extremely weakly supervision. Our key finding is that the pseudo labels can be constructed by learning the local relationship among geophysical properties at very sparse locations. We explore a multi-physics inversion problem from two distinct measurements (seismic and EM data) to three geophysical properties (velocity, conductivity, and CO₂ saturation). Our results show that we are able to invert for properties without explicit governing equations. Moreover, the label data on three geophysical properties can be significantly reduced by 50 times (from 100 down to only 2 locations).

1. Introduction

Geophysical properties (such as velocity, conductivity and CO₂ saturation) provide structural and numerical information for various geophysical applications, e.g. assessment of oil and gas reservoirs and sequestration of CO₂ (Lucia et al., 2003). These properties are obtained from surface-based geophysical measurements including seismic (Yilmaz, 2001), electromagnetics (EM) (Zhdanov, 2009), gravity (Li & Oldenburg, 1998), etc, by geophysical inversion.

These inversion problems have been studied *separately* (see Fig. 2) along two directions: physics-driven and data-

¹Los Alamos National Laboratory ²Microsoft. Correspondence to: Shihang Feng <shihang.feng@live.com>, Youzuo Lin <yulin@lanl.gov>.

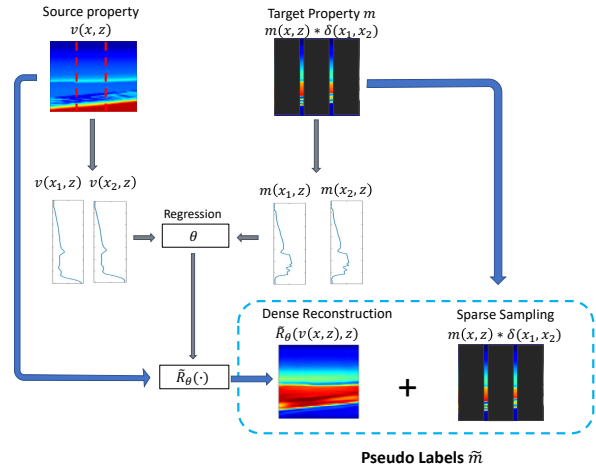


Figure 1. Schematic illustration of our proposed method, which generate the pseudo labels \tilde{m} from the sparse samplings of the target property m and the full labeling of the source property v .

driven. The physics-driven methods (Zhdanov et al., 2000; Virieux & Operto, 2009; Feng & Schuster, 2017; 2019; Chen et al., 2020; Feng et al., 2021a) are applicable for seismic \rightarrow velocity and EM \rightarrow conductivity by leveraging the known PDE, which is converted as a forward modeling operator such that the input (seismic or EM) is a function of output (velocity or conductivity). Based on the forward modeling, velocity and conductivity can be iteratively optimized. The data-driven methods apply to the inversion problems by leveraging deep neural networks to learn a correspondence from geophysical measurements to geophysical properties (Araya-Polo et al., 2018; Wu & Lin, 2019; Jin et al., 2020; Feng et al., 2021b). This type of works require a large amount of paired geophysical measurements and geophysical properties to train the network.

Jointly inverting multiple geophysical data simultaneously collected from the same area can improve the estimation of geophysical properties and reduce the uncertainty (Hu et al., 2021). The joint multi-physics inversion has been widely studied in the physics-driven methods with the properties explicitly governed by the PDEs (such as velocity and conductivity) (Hoversten et al., 2003; Lelièvre et al., 2012). But the physics-driven methods are unable to invert properties

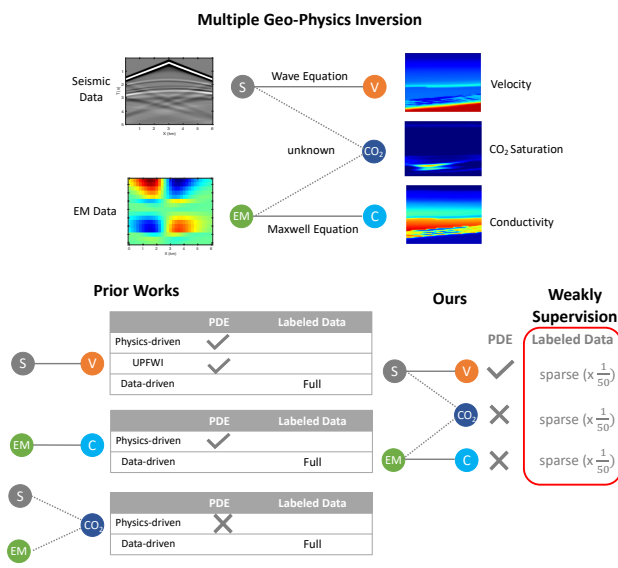


Figure 2. Schematic illustration of the Weakly Supervised Multiple Geo-Physics Inversion (WS-MGI) and the comparison with the prior works.

without explicit governing equations (such as CO_2 saturation) since the gradient in the iterative optimization can not be solved.

Properties without explicit governing equations can be obtained with the supervised data-driven methods. However, the acquisition of the labelled data is extremely expensive, only sparse labelled data can be acquired in the field experiments. (Sun et al., 2020) firstly present a joint inversion that reconstruct salt geometry by combining seismic and electromagnetic data, but it still rely on large amount of labelled data, which is impossible to be obtained in the real case.

In this work, we shift the data-driven inversion paradigm to *jointly* address these three inversion problems with *extremely weak* supervision (see Fig. 2). The three inversion problems are as follows: (a) seismic \rightarrow velocity to recover velocity maps from seismic data, (b) EM \rightarrow conductivity to recover conductivity maps from EM data, and (c) seismic/EM \rightarrow CO_2 to recover CO_2 saturation maps from seismic and EM data. The first two are governed by partial differential equations (wave and Maxwell's equation), while the physics for the last one is unknown. Only $\frac{1}{50}$ samplings in the maps are labelled. We propose a two-stage solution for these problem. In the first step, a single-physics inversion is preformed in an unsupervised way. In the second step, we construct the pseudo labels by approximating the relationship between the geophysical properties, which enable the inversion of the properties that do not have explicit governing equa-

tions. The requirement of the multi-physics labelled data is greatly reduced. We name our multi-physics method as Weakly Supervised Multiple Geo-Physics Inversion (WS-MGI) and evaluate our methodology on the Kimberlina reservoir data (Alumbaugh et al., 2021). These numerical results demonstrate that WS-MGI can accurately reconstruct the subsurface structures with sparse labelled data.

2. Backgrounds and Related Works

Geophysical survey collects the multi-physics data to extract useful information about the geophysical properties. Geophysical forward modeling can be posted as

$$\mathbf{d} = f(\mathbf{m}), \quad (1)$$

where \mathbf{d} is the geophysical measurement, \mathbf{m} is the geophysical properties and f is the geophysical forward modeling operator.

Some of the forward modeling operator f is governed by the PDEs. For example, The velocity maps and seismic measurements are correlated through an acoustic-wave equation as follows (Schuster, 2017):

$$\nabla^2 p(\mathbf{r}, t) - \frac{1}{v^2(\mathbf{r})} \frac{\partial^2 p(\mathbf{r}, t)}{\partial t^2} = s(\mathbf{r}, t), \quad (2)$$

where $v(\mathbf{r})$ is the velocity at spatial location \mathbf{r} , $\nabla^2 = \left(\frac{\partial^2}{\partial x^2} + \frac{\partial^2}{\partial z^2} \right)$ is the Laplacian operator in 2D Cartesian coordinates, $s(\mathbf{r}, t)$ is the source term, $p(\mathbf{r}, t)$ is the pressure data, and t represents time.

In the similar way, the conductivity map and EM measurements are correlated through the Maxwell's equations as follows (Commer & Newman, 2008):

$$\begin{aligned} \sigma \mathbf{E} - \nabla \times \mathbf{H} &= -\mathbf{J}, \\ \nabla \times \mathbf{E} + i\omega\mu_0 \mathbf{H} &= -\mathbf{M}, \end{aligned} \quad (3)$$

where \mathbf{H} and \mathbf{E} are the magnetic and electric fields, respectively. \mathbf{J} and \mathbf{M} are the electric and magnetic sources. σ is the electrical conductivity and μ_0 is the magnetic permeability of free space that $\mu_0 = 4\pi \times 10^{-7}$ ohm-seconds per meter.

Given the forward modeling operator f , the physics-driven method invert the geophysical properties \mathbf{m} by minimizing the loss function:

$$l_{\text{geo}} = \frac{1}{2} \sum ||f(\mathbf{m}) - \mathbf{d}||^2. \quad (4)$$

But for some geophysical properties, such as CO_2 saturation, are not connected with the surface-based geophysical

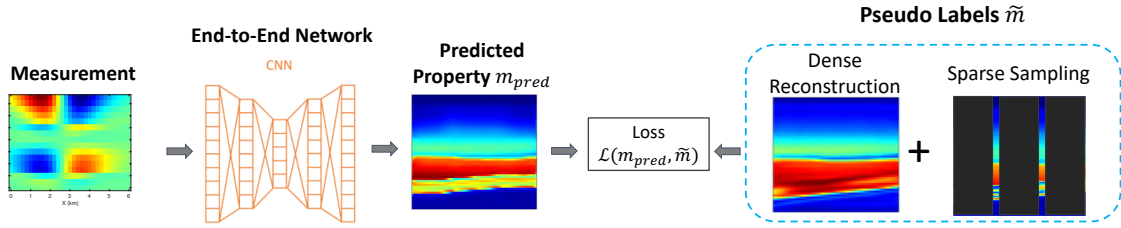


Figure 3. Schematic illustration of the encoder-decoder trained with the pseudo labels.

measurements by PDEs and f is unknown. The physics-driven methods are not feasible for such properties (see Fig. 2).

In the data-driven methods, convolutional neural networks $g(\cdot)$ are trained to approximate the inverse mapping $f^{-1}(\cdot)$ from geophysical measurement \mathbf{d} to geophysical properties \mathbf{m} whether f is known:

$$\mathbf{m} = g(\mathbf{d}) \approx f^{-1}(\mathbf{d}). \quad (5)$$

Such methods are able to invert for all the geophysical properties with the requirement of paired geophysical measurement \mathbf{d} and labelled geophysical properties \mathbf{m} for the training.

The accurate labelled geophysical properties can only be obtained from well logs, which are collected by the instruments lowered in a borehole that is penetrating the geologic formations (Ellis & Singer, 2007). The borehole is drilled vertically aiming at a target directly below the surface (Ma et al., 2016). The drilling is very expensive and only a few boreholes are drilled in the field experiments (Bassiouni et al., 1994; Lukawski et al., 2014), so that the labelled properties are always sparse.

Pseudo Labels in Computer Vision vs. Geophysics

In this paper, we have used pseudo labels to enable the multi-physics data-driven inversion of properties and overcome the sparse sampling problem in geophysics. Notice that there are differences between the pseudo labels in our problems and those in Computer Vision.

Pseudo labels are used on the semi-supervised learning in the Computer Vision area (Lee et al., 2013). The network is initially trained with a small set of labelled data. Then the confident predicted test data is added to the training data as the pseudo label to fine-tune the network. The building of the pseudo labels is based on the information from the same type of momentum.

In our methods with geophysics, the building of pseudo labels is based on its relationships with the other geophysical properties, which are the other types of momentum. More-

over, there are no existing small labelled data set for the initial training. Only sparse labelled data are available.

3. Methods

Multiple Geo-physics Inversion of the properties (such as CO₂ saturation) without explicit governing equations can only be achieved by supervised data-driven methods in the previous works. These methods are not feasible in the real cases since the collection of the labelled data is too expensive. Only sparse labelled data are available in the field, a weakly supervised data-driven inversion method is required for solving the multi-physics inversion.

3.1. Weakly Supervised Multiple Geo-physics Inversion

Here we proposed a Weakly Supervised Multiple Geo-physics Inversion (WS-MGI) method to invert multi-physics properties (source property v and target property m) with sparse samplings. The samplings are well logs $m(x = x_k, z)$, where x_k is the drilling location. The source property v is a property related to the geophysical measurements with PDEs while the target property m is the property without explicit governing equations. WS-MGI is implemented in two stages:

Stage 1: Invert for source property v from the geophysical measurements using an unsupervised method.

Stage 2: With the sparse sampling of target property $m(x = x_k, z)$ and the inverted source property at the corresponding location $v(x = x_k, z)$, we generate the pseudo labels \tilde{m} and train an end-to-end network with \tilde{m} to learn the mapping from geophysical measurement to m (Fig. 3). The trained network is then applied on the measurement to invert m .

3.2. Two-stage Solution

Stage 1. Unsupervised Single Geophysical Inversion: Stage 1 is an unsupervised inversion for single geophysical property v , which had already been proposed by Jin

et al. (2021) as Unsupervised Physical-Informed Full Waveform Inversion (UPFWI) for velocity maps as v . However, the unsupervised learning methods are still unavailable for other geophysical properties, such as conductivity and CO₂ saturation. UPFWI connects the PDE and neural neural to obtain the velocity map in an unsupervised way. The details of UPFWI are given in the Appendix.

Stage 2. Pseudo Labels Building and Training: To build the pseudo labels in Stage 2, we construct a simple regression model \tilde{R} using support vector regression (SVR) with Gaussian Kernel. The sparse sampling $m(x = x_k, z)$ and v at its corresponding location $v(x = x_k, z)$ are discretized into N training samples:

$$\left(\begin{pmatrix} v^{(i)} \\ z^{(i)} \end{pmatrix}, m^{(i)} \right), \quad (6)$$

where $i = 1, 2, \dots, N$. The model $\tilde{R}_\theta(\cdot)$ is trained by minimizing

$$\sum_N \left\{ \tilde{R}_\theta(v^{(i)}, z^{(i)}) - m^{(i)} \right\}, \quad (7)$$

and applied on $v(x, z)$ to obtain the dense reconstruction $\tilde{R}_\theta(v(x, z), z)$. The dense reconstruction provides the global information of m , but it is inaccurate due to the simplification of the rock-physics model. To account for the inaccuracy, we add the well log data $m(x = x_k, z)$ as the sparse sampling and combine it the dense reconstruction to composite the pseudo label:

$$\tilde{m}(x, z) = \lambda_1 \overbrace{\tilde{R}_\theta(v(x, z), z)}^{\text{dense reconstruction}} + \lambda_2 \overbrace{\sum_i m(x, z) * \delta(x_k)}^{\text{sparse sampling}} \quad (8)$$

where λ_1 and λ_2 are the weight for dense reconstruction and sparse sampling. The dense reconstruction provides the global but inaccurate information while the sampling provides the accurate but local information.

The end-to-end network takes the geophysical measurements, such as seismic and EM data, as the inputs and generate geophysical properties m_{pred} (see Fig. 3). With the pseudo labels \tilde{m} , the network g can be trained with the loss function $\mathcal{L}(m_{pred}, \tilde{m})$ to approximate the inverse mapping $f^{-1}(\cdot)$ as in Eq. 5.

In this paper, we set velocity map as the source property v and it can be learned from the seismic data by UPFWI without labeling. Although WS-MGI is designed for m as the property without explicit governing equations, m can also be a property explicitly governed by PDEs. We choose m to be CO₂ saturation and conductivity to validate the effectiveness of this method.

4. Experiments

In this section, we apply this method on the Kimberlina reservoir dataset. The original geophysical properties was developed under DOE's National Risk Assessment Program (NRAP) based on a potential CO₂ storage site in the Southern San Joaquin Basin of California (Alumbaugh et al., 2021). To the best of our knowledge, it is the largest data set for the multi-physics study in the geophysics area. In this data, there are 780 samples and each sample contains a set of seismic and EM data as geophysical measurements, velocity, conductivity and CO₂ saturation maps as properties and two well log data that provides CO₂ saturation and conductivity. In our experiments, 750 samples are set as training set and the rest are the validation set.

4.1. Kimberlina Data

The saturation maps and velocity maps are with the size of $59 \times 100 (H \times W)$, where H and W are the depth and the width of the maps. The grid is 60 m in all dimensions. Two well logs are located at 2 km and 4 km.

There are 5 seismic sources serving as stimulus placed evenly on the 2D spatial grid over the surface with a shot interval of 1.2 m. Seismic data are simulated using the finite-difference method (Moczo et al., 2007). Each of them captures vibration signals as time-series data of length 1,001 with a time spacing of 0.005 s. Both the seismic and EM data are collected by 100 receivers uniformly distributed over the 2D earth surface with a receiver interval of 60 m. The size of seismic data is $5 \times 1000 \times 100 (S \times T \times R)$, where S and R are the number of sources and receivers, T is the time steps.

EM data are simulated by finite-difference method (Commer & Newman, 2008) with two sources location at $x = 2.5$ km, $z = 3.025$ km and $x = 4.5$ km, $z = 2.5$ km. There are 8 source frequencies from 0.1 to 8.0 Hz and the data with each frequency has a real part and a imaginary part. Since EM data do not have the time axis, its size is $(2 \times 16 \times 100) (S \times F \times R)$, where F is the number of the frequencies. The detailed images of the seismic and EM data are given in the Appendix.

4.2. Workflow

Stage 1: The velocity maps are provided by UPFWI as in Fig. 4a. The resolution of the UPFWI velocity maps is lower than the true velocity maps due to the limitation of the frequency in full waveform inversion (Schuster, 2017).

Stage 2: We use two well logs at $x = 2$ km and $x = 4$ km as the sparse samplings ($\frac{1}{50} \times$ full labels) and the UPFWI velocity maps (see Fig. 5) at the corresponding location in the training of SVR to predict the dense reconstructions.

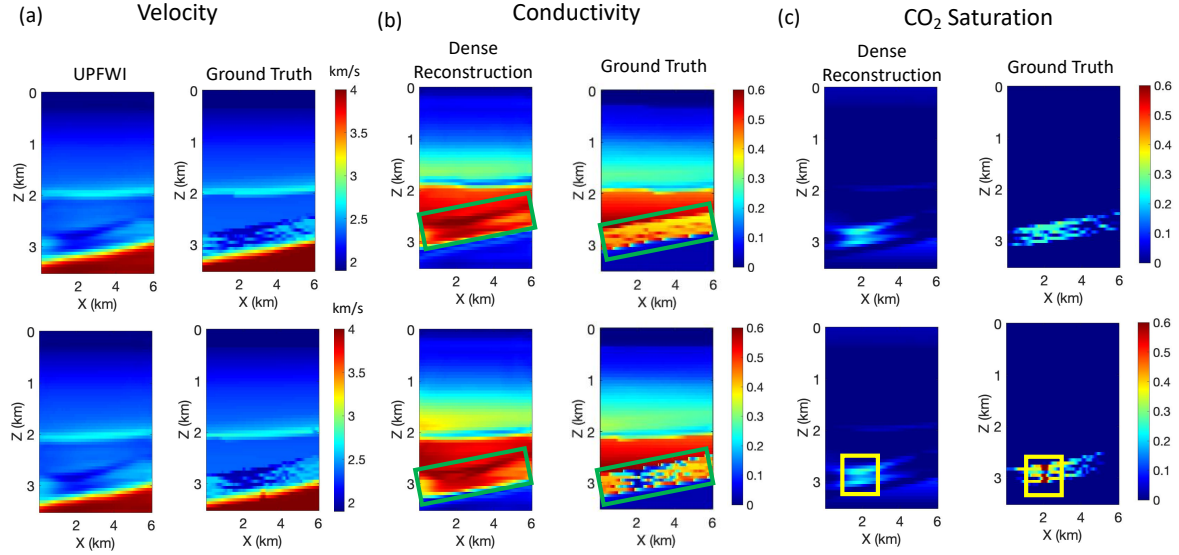


Figure 4. (a) Velocity maps given by UPFWI. (b) Conductivity dense reconstruction and true conductivity map. (c) CO_2 saturation dense reconstruction and true CO_2 saturation map.

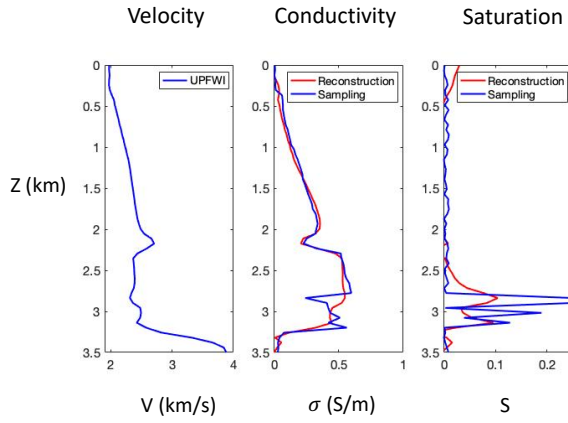


Figure 5. Examples of profiles: the velocity profile provided by UPFWI, the sparse samplings provided by well logs and the dense reconstructions provided by SVR of conductivity and CO_2 saturation maps.

The predicted dense reconstructions are shown in Figs. 4b and 4c and their vertical profiles are shown in Fig. 5. We can see the dense reconstruction are inaccurate, especially the reservoir area in conductivity map (see Green boxes in Fig. 4b) and the high saturation area in CO_2 saturation map (see Yellow boxes in Fig. 4c). Then we combine the inaccurate dense reconstructions and the accurate sparse samplings to construct pseudo labels with Eq. (8). The pseudo labels are fed into an end-to-end network g to learning the mapping from the seismic and EM data to conductivity and CO_2

saturation as in Eq. (5).

4.3. Implement Details

Training Details: The input seismic and EM data are normalized into range $[-1, 1]$. We employ Adam optimizer with momentum parameters $\beta_1 = 0.5$ and $\beta_2 = 0.999$. The learning rate is set to be 1×10^{-4} and it gradually decrease with the increasing of epoch number. The size of mini-batch is set to be 10. The ℓ_1 loss function is used in the training. We implement our models in Pytorch and train them on a Tesla V100 GPU with 50 epochs. All models are randomly initialized.

Networks: The measurement (seismic and EM data) and the properties (conductivity and CO_2 saturation) are connected by an encoder-decoder network. The encoder with seismic data as the input has 7 convolutional layers (with stride 2 every the other layer to reduce dimension) and the encoder with EM data as the input has 5 convolutional layers. The decoder is 4 convolutional layers with nearest neighbor upsampling in between following a center-cropping of the feature map and a convolution layer to output the property map. If both seismic and EM data are used as inputs, they are fed into two parallel the encoders and then concatenated in the latent spaces.

Evaluation Metrics: The mean-square errors (MSE), mean-absolute errors (MAE), and Structural Similarity (SSIM) are used for the evaluating the conductivity and saturation. MSE and MAE are widely used in the existing geophysical inversion methods (Araya-Polo et al., 2018; Wu & Lin,

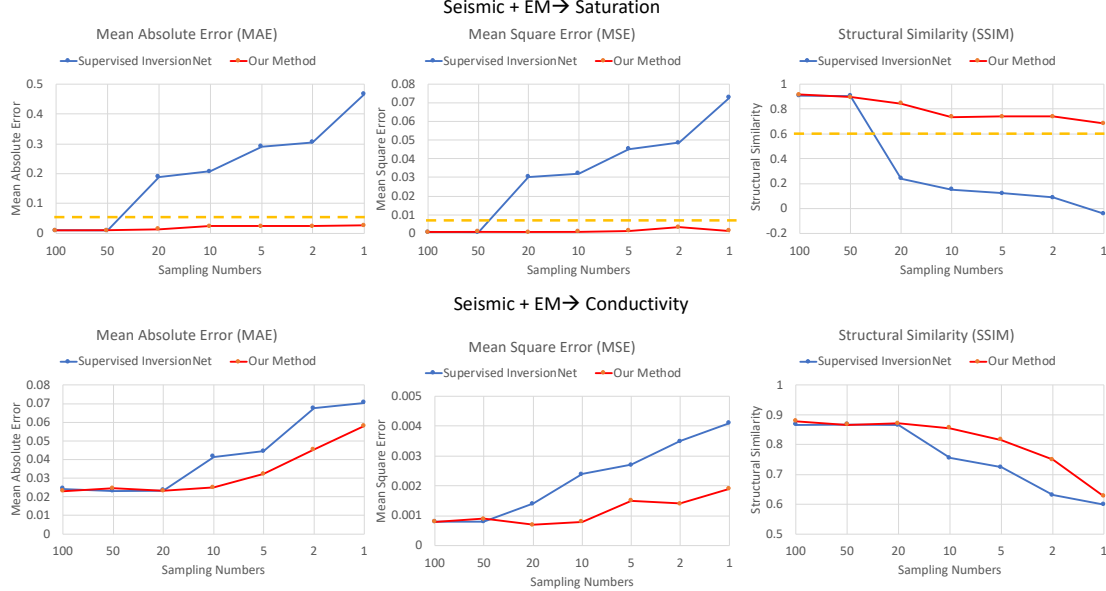


Figure 6. Weakly Supervised Multiple Geo-physics Inversion (ours) vs. Supervised InversionNet (Wu & Lin, 2019). Our method achieves better performance e.g. lower Mean Absolute Error (MAE) and higher Structural Similarity (SSIM).

2019). The high-level structure in the geological formation can be easily distinguished by human vision. To better align with the human vision, we use SSIM as one of our evaluation metrics (Jin et al., 2021).

Comparison: There are no existing inversion methods designed specifically for the inversion with sparse labeling, we compare our methods with the supervised InversionNet method (Wu & Lin, 2019; Zeng et al., 2021). The structure of the end-to-end network in the InversionNet is the same with our method. There are totally 100 samples for the full label, we gradually decrease the number of samples and evaluate the performance of the methods when the sampling become more and more sparse.

4.4. Main Results

Fig. 6 compares the results with the supervised InversionNet and our method on two scenarios:

Seismic+EM→CO₂ Saturation: In this scenario, Seismic and EM data are set as the input measurement and the target property m is CO₂ Saturation. The ratio between the weight λ_1 and λ_2 is set as 1. When the sampling number is less than 20 ($\frac{1}{5} \times$ full labels), the performance of the InversionNet quickly degrades, the MAE become higher than 0.2, MSE increase to 0.03 and SSIM decrease to 0.2. But our method always keeps MAE less than 0.05, MSE less than 0.01 and SSIM higher than 0.6. Examples of the results are shown in Fig. 7. The saturation maps given by InversionNet contain

large amount of artifacts in the background. The results with our WS-MGI method is consistent with the ground truth. Moreover, the high saturation zone in the yellow box is inverted clearly.

Seismic+EM→Conductivity: In this scenarios, seismic and EM data are the input measurement and the target property m is conductivity. The ratio between the weight λ_1 and λ_2 is set as 10. The relationship between the conductivity and EM data is govern by the PDE. When sampling number decreases, the performance of InversionNet decreases slower than the saturation. However, our methods still have lower MAE, lower MSE and higher SSIM than those of the InversionNet for all the sampling numbers. In Fig. 7, the thin layers in the blue boxes are reconstructed much better in our result than the one obtained using InversionNet.

5. Ablation Study

In this section, we discuss different factors that affect the performance of our method. Five tests are studied below and more results are given in the Appendix.

5.1. The Inversion Scenarios

We have test 5 different scenarios, of which conductivity and saturation are inverted from EM and seismic data. For each scenario, we compare the results with different labels (sparse sampling, dense reconstruction and pseudo label Eq. (8)) as the training labels for the network. The inversion

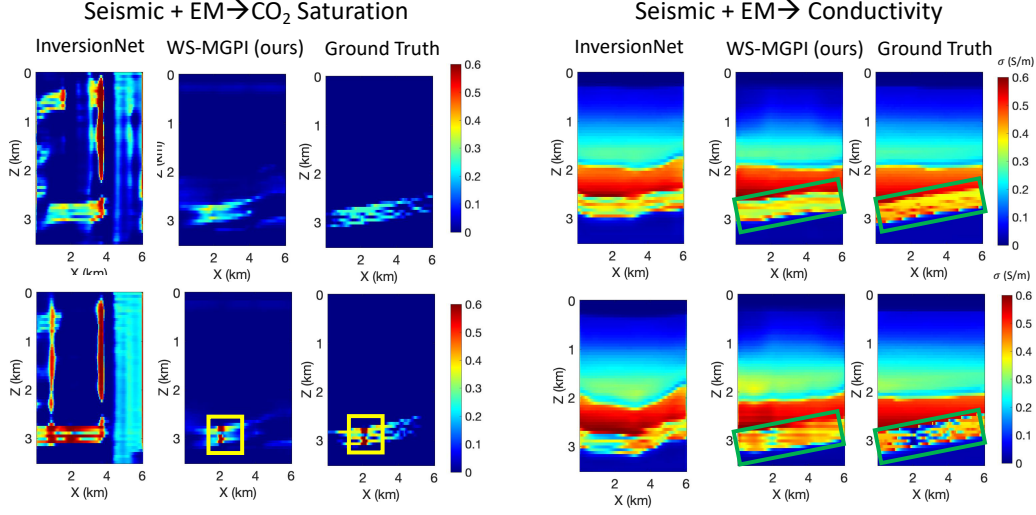


Figure 7. Comparison of InversionNet and WS-MGI (ours) on inverted CO_2 saturation and conductivity maps when sampling number equal to 2.

Table 1. Quantitative results with different label setting in different inversion scenarios

		MAE \downarrow	MSE \downarrow	SSIM \uparrow
Seismic \rightarrow Saturation	Sampling	0.1603	0.0520	0.2554
	Reconstruction	0.0271	0.0037	0.6837
	Pseudo	0.0175	0.0022	0.7911
EM \rightarrow Saturation	Sampling	0.5318	0.1678	-0.0150
	Reconstruction	0.0229	0.0028	0.7147
	Pseudo	0.0222	0.0028	0.7273
{EM Seismic} \rightarrow Saturation	Sampling	0.2449	0.0771	0.1691
	Reconstruction	0.0273	0.0037	0.6844
	Pseudo	0.0193	0.0034	0.7388
EM \rightarrow Conductivity	Sampling	0.0523	0.0031	0.7019
	Reconstruction	0.0664	0.0029	0.5858
	Pseudo	0.0450	0.0015	0.7126
{EM Seismic} \rightarrow Conductivity	Sampling	0.0519	0.0030	0.6921
	Reconstruction	0.0691	0.0029	0.5792
	Pseudo	0.0452	0.0024	0.7388

with sparse sampling would be the same with the supervised learning with sparse labeling. Their quantitative results are listed in Table 1 and examples of the results are given in the Appendix. For the inversion of conductivity, the sparse sampling can give a reasonable result while it can only provide poor results for the inversion of CO_2 saturation. Among all the scenarios, the performance of the pseudo labels is always the best.

5.2. The Choosing of Weight Ratio

The selection of the weight in Eq. (8) is important in the construction of the pseudo label. We have tested our methods with different weight setting. The results are given in Table 2. For the inversion of conductivity, the sparse sampling has a good regularization on the inversion result. It has the

Table 2. The MAE, MSE and SSIM losses with Different Weight Ratio λ_1/λ_2

	Weight Ratio λ_1/λ_2	MAE \downarrow	MSE \downarrow	SSIM \uparrow
{EM Seismic} \rightarrow Saturation	0.1	0.0251	0.0016	0.7327
	0.2	0.0242	0.0014	0.7444
	0.5	0.0243	0.0015	0.7416
	1	0.0239	0.0014	0.7486
	2	0.0249	0.0016	0.7182
	5	0.0246	0.0016	0.7343
	10	0.0255	0.0016	0.6980
	Weight Ratio λ_1/λ_2	MAE \downarrow	MSE \downarrow	SSIM \uparrow
	0.1	0.0452	0.0024	0.7388
	0.2	0.0578	0.0021	0.6362

	Weight Ratio λ_1/λ_2	MAE \downarrow	MSE \downarrow	SSIM \uparrow
{EM Seismic} \rightarrow Conductivity	0.1	0.0599	0.0024	0.6203
	0.2	0.0610	0.0024	0.6162
	0.5	0.0617	0.0023	0.6059
	1	0.0616	0.0024	0.6095
	2	0.0611	0.0024	0.6171
	5			
	10			
	Weight Ratio λ_1/λ_2	MAE \downarrow	MSE \downarrow	SSIM \uparrow
	0.1			
	0.2			

best results when the sparse sampling has a higher weight $\lambda_1/\lambda_2 = 0.1$. For saturation, a balanced weight $\lambda_1/\lambda_2 = 1$ would be the best option.

5.3. The Accuracy of Dense Reconstruction

The dense reconstruction in Eq. (8) is obtained by the Gaussian Kernel Regression from the sparse sampling in WS-MGI and its accuracy would affect the inversion results. To study the influence of the dense reconstruction on the results, we apply different Gaussian filters on the ground truth to approximate dense reconstructions in different accuracy. Table 3 shows the results with the smoothed ground truth as the dense reconstructions. With the increasing of the σ value in the filter, the accuracy of the dense reconstruction

Table 3. The MAE, MSE and SSIM losses with Different Smoothed Ground Truth as Dense Reconstruction

		Gaussian Filter	MAE \downarrow	MSE \downarrow	SSIM \uparrow
		σ			
$\left\{ \begin{array}{l} \text{EM} \\ \text{Seismic} \end{array} \right\} \rightarrow \text{Saturation}$	0.5	0.0075	0.0006	0.9443	
	1	0.0121	0.0011	0.8778	
	3	0.0151	0.0011	0.8535	
	5	0.0173	0.0009	0.8412	
$\left\{ \begin{array}{l} \text{EM} \\ \text{Seismic} \end{array} \right\} \rightarrow \text{Conductivity}$	Gaussian Filter		MAE \downarrow	MSE \downarrow	SSIM \uparrow
	σ				
	0.5	0.0294	0.0013	0.8149	
	1	0.0326	0.0326	0.8081	
	3	0.0408	0.0008	0.7488	
	5	0.0517	0.0013	0.6968	

Table 4. The MAE, MSE and SSIM losses with Different Noise Level

		SNR	MAE \downarrow	MSE \downarrow	SSIM \uparrow
$\left\{ \begin{array}{l} \text{EM} \\ \text{Seismic} \end{array} \right\} \rightarrow \text{Saturation}$	40	0.0249	0.0015	0.7317	
	30	0.0251	0.0015	0.7144	
	20	0.237	0.0014	0.7449	
	10	0.0256	0.0019	0.7227	
	0	0.0295	0.0023	0.6468	
	-10	0.0310	0.0024	0.6293	
	-20	0.0300	0.0024	0.6558	
	-30	0.0306	0.0024	0.6462	
$\left\{ \begin{array}{l} \text{EM} \\ \text{Seismic} \end{array} \right\} \rightarrow \text{Conductivity}$	SNR	MAE \downarrow	MSE \downarrow	SSIM \uparrow	
	40	0.0471	0.0026	0.7241	
	30	0.0471	0.0026	0.7243	
	20	0.0469	0.0026	0.7250	
	10	0.0414	0.0052	0.7798	
	0	0.0412	0.0052	0.7794	
	-10	0.0455	0.0064	0.7414	
	-20	0.0639	0.0113	0.6389	
	-30	0.1030	0.0210	0.5013	

decrease. As a result, the performance of the WS-MGI would also decrease.

5.4. Robustness to Noise

The geophysical measurement, seismic data and EM data, collected in the field contain the noise of certain levels. To demonstrate the robustness of the proposed WS-MGI methods against noise, we impose random noise in the measurements and test the WS-MGI model under different signal-to-noise ratio (SNR). Table 4 shows the results of this experiment, from which it can be observed that WS-MGI with conductivity maintains competitive performance until SNR = -10 dB and WS-MGI with CO₂ saturation keeps good performance until SNR = 0 dB. However, real-world environment with a constant negative SNR is rare and thus it is shown that WS-MGI is robust to noise in typical application scenarios.

5.5. Missing Traces in the Measurements

In the geophysical field experiments, there are always trace missing in acquired measurements because of existing obstacles and economic restrictions (Wang et al., 2019). The

Table 5. The MAE, MSE and SSIM losses with Missing Traces in the Measurements

		Missing Traces (%)	MAE \downarrow	MSE \downarrow	SSIM \uparrow
		30	0.0256	0.0017	0.7257
		60	0.0267	0.0018	0.7186
		90	0.0300	0.0040	0.6935
		Missing Traces (%)	MAE \downarrow	MSE \downarrow	SSIM \uparrow
		30	0.0475	0.0026	0.7178
		60	0.0552	0.0030	0.6641
		90	0.0678	0.108	0.6101

robustness of the network with the missing traces would be crucial for the application in the real cases. We test our methodology on data with missing traces as in Table 5. The performance of the WS-MGI gradually decrease when the available data become less.

6. Conclusions

In this paper, we proposed Weakly Supervised Multiple Geo-Physics Inversion (WS-MGI) that solve multi-physics inversion problem with sparse samplings. With pseudo labels built from the sparse labeling of the properties, we are able to train an end-to-end network that learn the mapping from the measurement to the property. This network enable the inversion of geophysical properties that only have an implicit relationship with the measurement. Moreover, solving the multi-physics inversion in a weakly supervised way saves the extremely high cost of the label collection, which is much more practical than the previously existing supervised inversion methods.

We successfully implement this method with Kimberline data on the inversion of CO₂ saturation and conductivity. Compared with the supervised inversion methods that requires at least 20 samplings ($\frac{1}{5} \times$ full labels), WS-MGI successfully reconstruct the geological structures and CO₂ saturation with only 2 well logs as the sparse samplings ($\frac{1}{50} \times$ full labels).

References

- Alumbaugh, D., Commer, M., Crandall, D., Gasperikova, E., Feng, S., Harbert, W., Li, Y., Lin, Y., Manthila Samarasringhe, S., and Yang, X. Development of a multi-scale synthetic data set for the testing of subsurface CO₂ storage monitoring strategies. In *American Geophysical Union (AGU 2021)*, 2021.
- Araya-Polo, M., Jennings, J., Adler, A., and Dahlke, T. Deep-learning tomography. *The Leading Edge*, 37(1): 58–66, 2018.
- Bassiouni, Z. et al. *Theory, measurement, and interpretation of well logs*, volume 4. Henry L. Doherty Memorial Fund of AIME, Society of Petroleum Engineers, 1994.

Chen, Y., Feng, Z., Fu, L., AlTheyab, A., Feng, S., and Schuster, G. Multiscale reflection phase inversion with migration deconvolution. *Geophysics*, 85(1):R55–R73, 2020.

Commer, M. and Newman, G. A. New advances in three-dimensional controlled-source electromagnetic inversion. *Geophysical Journal International*, 172(2):513–535, 2008.

Ellis, D. V. and Singer, J. M. *Well logging for earth scientists*, volume 692. Springer, 2007.

Feng, S. and Schuster, G. T. Skeletonized wave-equation inversion in vertical symmetry axis media without too much math. *Interpretation*, 5(3):SO21–SO30, 2017.

Feng, S. and Schuster, G. T. Transmission+ reflection anisotropic wave-equation traveltime and waveform inversion. *Geophysical Prospecting*, 67(2):423–442, 2019.

Feng, S., Fu, L., Feng, Z., and Schuster, G. T. Multiscale phase inversion for vertical transverse isotropic media. *Geophysical Prospecting*, 69(8-9):1634–1649, 2021a.

Feng, S., Lin, Y., and Wohlberg, B. Multiscale data-driven seismic full-waveform inversion with field data study. *arXiv preprint arXiv:2103.04007*, 2021b.

Hoversten, G. M., Gritto, R., Washbourne, J., and Daley, T. Pressure and fluid saturation prediction in a multicomponent reservoir using combined seismic and electromagnetic imaging. *Geophysics*, 68(5):1580–1591, 2003.

Hu, Y., Wei, X., Wu, X., Sun, J., Chen, J., Chen, J., and Huang, Y. Deep learning-enhanced multiphysics joint inversion. In *First International Meeting for Applied Geoscience & Energy*, pp. 1721–1725. Society of Exploration Geophysicists, 2021.

Jin, P., Feng, S., Lin, Y., Wohlberg, B., Moulton, D., Cromwell, E., and Chen, X. Cyclefcn: A physics-informed data-driven seismic waveform inversion method. In *SEG Technical Program Expanded Abstracts 2020*, pp. 3867–3871. Society of Exploration Geophysicists, 2020.

Jin, P., Zhang, X., Chen, Y., Huang, S. X., Liu, Z., and Lin, Y. Unsupervised learning of full-waveform inversion: Connecting cnn and partial differential equation in a loop. *arXiv preprint arXiv:2110.07584*, 2021.

Lee, D.-H. et al. Pseudo-label: The simple and efficient semi-supervised learning method for deep neural networks. In *Workshop on challenges in representation learning, ICML*, volume 3, pp. 896, 2013.

Lelièvre, P. G., Farquharson, C. G., and Hurich, C. A. Joint inversion of seismic traveltimes and gravity data on unstructured grids with application to mineral exploration. *Geophysics*, 77(1):K1–K15, 2012.

Li, Y. and Oldenburg, D. W. 3-d inversion of gravity data. *Geophysics*, 63(1):109–119, 1998.

Lucia, F. J., Kerans, C., and Jennings, J. W. Carbonate reservoir characterization. *Journal of Petroleum Technology*, 55(06):70–72, 2003.

Lukawski, M. Z., Anderson, B. J., Augustine, C., Capuano Jr, L. E., Beckers, K. F., Livesay, B., and Tester, J. W. Cost analysis of oil, gas, and geothermal well drilling. *Journal of Petroleum Science and Engineering*, 118:1–14, 2014.

Ma, T., Chen, P., and Zhao, J. Overview on vertical and directional drilling technologies for the exploration and exploitation of deep petroleum resources. *Geomechanics and Geophysics for Geo-Energy and Geo-Resources*, 2(4):365–395, 2016.

Moczo, P., Robertsson, J. O., and Eisner, L. The finite-difference time-domain method for modeling of seismic wave propagation. *Advances in geophysics*, 48:421–516, 2007.

Schuster, G. T. *Seismic inversion*. Society of Exploration Geophysicists, 2017.

Sun, Y., Denel, B., Daril, N., Evano, L., Williamson, P., and Araya-Polo, M. Deep learning joint inversion of seismic and electromagnetic data for salt reconstruction. In *SEG Technical Program Expanded Abstracts 2020*, pp. 550–554. Society of Exploration Geophysicists, 2020.

Virieux, J. and Operto, S. An overview of full-waveform inversion in exploration geophysics. *Geophysics*, 74(6):WCC1–WCC26, 2009.

Wang, B., Zhang, N., Lu, W., and Wang, J. Deep-learning-based seismic data interpolation: A preliminary result. *Geophysics*, 84(1):V11–V20, 2019.

Wu, Y. and Lin, Y. Inversionnet: An efficient and accurate data-driven full waveform inversion. *IEEE Transactions on Computational Imaging*, 6:419–433, 2019.

Yilmaz, Ö. *Seismic data analysis: Processing, inversion, and interpretation of seismic data*. Society of exploration geophysicists, 2001.

Zeng, Q., Feng, S., Wohlberg, B., and Lin, Y. Inversionnet3d: Efficient and scalable learning for 3d full waveform inversion. *arXiv preprint arXiv:2103.14158*, 2021.

Zhdanov, M. S. *Geophysical electromagnetic theory and methods*. Elsevier, 2009.

Zhdanov, M. S., Fang, S., and Hursán, G. Electromagnetic inversion using quasi-linear approximation. *Geophysics*, 65(5):1501–1513, 2000.

A. Appendix

A.1. Unsupervised physical-informed Full waveform inversion (UPFWI)

The illustration of UPFWI is shown in the Figure 8. An encoder-decoder structure is connected with the forward modeling of the seismic data to model the mapping from seismic data $\mathbf{p} \in \mathbb{R}^{S \times T \times R}$ to velocity map $\mathbf{v} \in \mathbb{R}^{H \times W}$. It is trained in an unsupervised way by minimizing l_{seis} :

$$l_{seis} = \frac{1}{2} \sum ||f_{seis}(\mathbf{v}) - \mathbf{p}||, \quad (9)$$

which where \mathbf{p} is the input seismic data, \mathbf{v} is the predicted velocity map, f_{seis} is the forward modeling operator is governed by the wave equation using a finite difference method (Moczo et al., 2007). The encoder is primary built with 7 convolutional layers (with stride 2 every the other layer to reduce dimension), which extract the high-dimensional features from the seismic data. The decoder projects the extracted features into velocity models through 4 convolutional layers with nearest neighbor upsampling in between. Finally we center-crop the feature map and apply a convolution layer to output the velocity map. The seismic data are normalized into range [-1,1] as the input. We employ Adam optimizer with momentum parameters $\beta_1 = 0.5$ and $\beta_2 = 0.999$. The learning rate is set to be 3×10^{-5} and it gradually decrease with the increasing of epoch number. The size of mini-batch is set to be 10. We implement UPFWI in Pytorch and train them on a Tesla V100 GPU with 250 epochs. The MSE, MAE and SSIM between the input and predicted seismic data and between the true and predicted velocity maps are listed in Table 6, which shows that the predicted velocity map given by UPFWI are accurate.

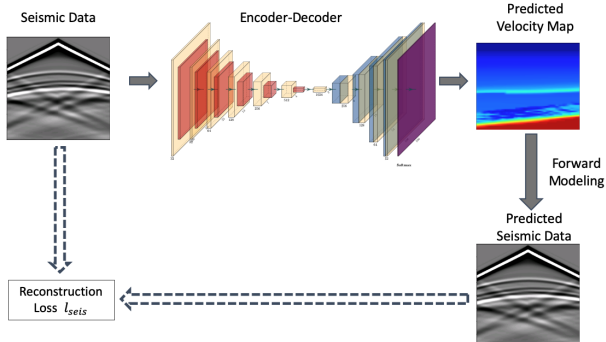


Figure 8. Schematic illustration of UPFWI, where trains an encoder-decoder to learn the mapping from seismic data to velocity maps.

Table 6. The MAE, MSE and SSIM losses with UPFWI results

Seismic Data Loss			Velocity Map Loss		
MAE	MSE	SSIM	MAE	MSE	SSIM
0.0275	0.0009	0.8909	0.0131	0.0008	0.9130

A.2. Geophysical Measurements

The examples of geophysical measurements are listed in Fig. 9. Seismic data has 5 sources and the data with different sources are aligned in different channels in the input of the neural network. EM data is simulated by two sources in 8 frequencies. The first 8 columns in the upper part are from the real part of the data and the 8 columns in the lower part are from the imaginary part.

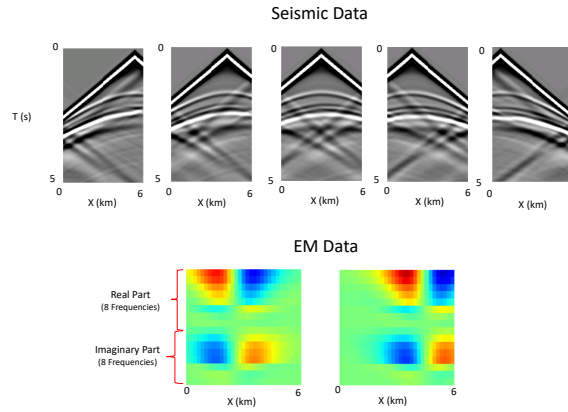


Figure 9. Examples of seismic and EM data.

A.3. Inversion Results

Table 7 and 8 show the quantitative results corresponding to two scenarios (Seismic+EM \rightarrow CO₂ saturation and Seismic+EM \rightarrow Conductivity) in Fig. 6.

We have studied 5 different scenarios from seismic and EM data to CO₂ saturation and conductivity in the ablation study. Examples of the results are listed in Fig. 10 and 11. For the inversion of CO₂ saturation, there is no constraint on the background when we only use the sparse sampling as the labels. There are lots of the artifacts in the background, especially the input data is EM data only since the size the EM data is much smaller than the seismic data. For the inversion of conductivity, the artifacts in the background are eliminated because of the constraint from the PDE.

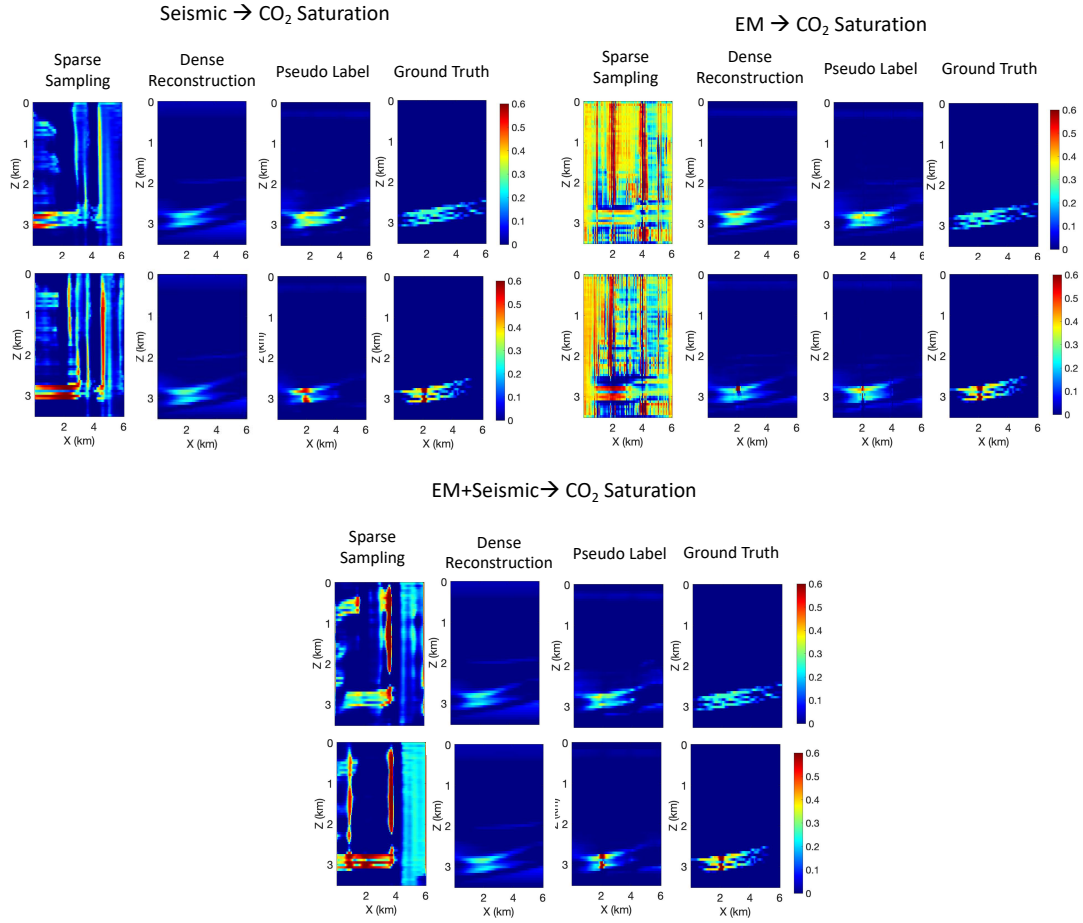


Figure 10. The comparison of inverted CO₂ saturation maps with different labels (sparse sampling only, dense reconstruction only and pseudo labels) and the ground truth from different scenarios.

Table 7. Comparison of WS-MGI (Ours) and InversionNet: the MAE, MSE and SSIM losses with Different Number of Sampling Labels (EM+seismic→Saturation)

		Sampling Labels Numbers	MAE↓	MSE↓	SSIM↑
WS-MGI (Ours)	{ EM Seismic }→Saturation	100	0.0104	0.0008	0.917
		50	0.0108	0.0009	0.8963
		20	0.015	0.0008	0.846
		10	0.0243	0.0009	0.7363
		5	0.0239	0.0013	0.7388
		2	0.0246	0.0034	0.7389
		1	0.0273	0.0015	0.6844
InversionNet	{ EM Seismic }→Saturation	Sampling Labels Numbers	MAE↓	MSE↓	SSIM↑
		100	0.0104	0.0008	0.9078
		50	0.0102	0.0007	0.9066
		20	0.1901	0.0303	0.2422
		10	0.2083	0.0321	0.154
		5	0.2916	0.0452	0.1228
		2	0.306	0.0486	0.0885
		1	0.4661	0.0727	-0.0411

Table 8. Comparison of WS-MGI (Ours) and InversionNet: the MAE, MSE and SSIM losses with Different Number of Sampling Labels (EM+seismic→Conductivity)

		Sampling Labels Numbers	MAE↓	MSE↓	SSIM↑
WS-MGI (Ours)	{ EM Seismic }→Conductivity	100	0.023	0.0008	0.878
		50	0.0246	0.0009	0.8664
		20	0.0231	0.0007	0.8701
		10	0.0249	0.0008	0.8553
		5	0.0323	0.0015	0.816
		2	0.0452	0.0014	0.7486
		1	0.058	0.0019	0.6266
InversionNet	{ EM Seismic }→Conductivity	Sampling Labels Numbers	MAE↓	MSE↓	SSIM↑
		100	0.0242	0.0008	0.8658
		50	0.0231	0.0008	0.8669
		20	0.0234	0.0014	0.8657
		10	0.0414	0.0024	0.7546
		5	0.0445	0.0027	0.7245
		2	0.0674	0.0035	0.631
		1	0.0703	0.0041	0.599

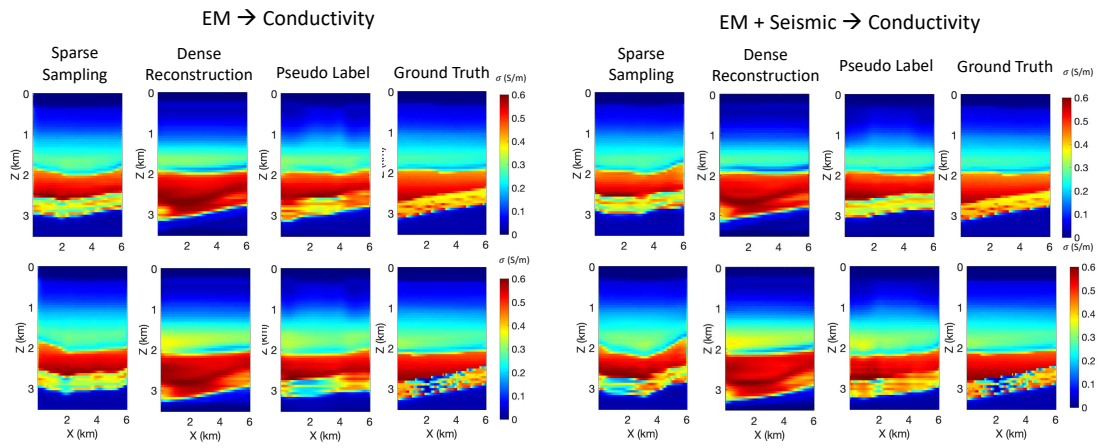


Figure 11. The comparison of inverted conductivity maps with different labels (sparse sampling only, dense reconstruction only and pseudo labels) and the ground truth from different scenarios.